Model for an indoor disturbed magnetic field

Nicolas Petit

▶ **To cite this version:**

Nicolas Petit. Model for an indoor disturbed magnetic field. [Research Report] Centre Automatique et Systèmes MINES ParisTech. 2015. hal-01220595

HAL Id: hal-01220595

https://minesparis-psl.hal.science/hal-01220595

Submitted on 26 Oct 2015

HAL is a multi-disciplinary open access archive for the deposit and dissemination of scientific research documents, whether they are published or not. The documents may come from teaching and research institutions in France or abroad, or from public or private research centers.

L'archive ouverte pluridisciplinaire **HAL**, est destinée au dépôt et à la diffusion de documents scientifiques de niveau recherche, publiés ou non, émanant des établissements d'enseignement et de recherche français ou étrangers, des laboratoires publics ou privés.

Model for an indoor disturbed magnetic field

Nicolas Petit
Centre Automatique et Systèmes
MINES ParisTech

The following document proposes a model for the magnetic field that can be measured indoor. The derivation of the parameters and of the model (along with necessary experiment conducted by ourselves) is detailed.

1 The Stationary Indoor Magnetic Field

One can define the time-independent magnetic field $\boldsymbol{B}_{stat}(\boldsymbol{X})$ which is supposed to be the stationary part of an indoor magnetic field. Mainly, this is nothing more than the local geomagnetic field disturbed and distorted by rebar steel, metal parts with ferromagnetic properties and permanent magnets [3],[1]. It is assumed that it can be described by :

$$\begin{aligned} B_{X,stat}(\boldsymbol{X}) &= f_{B_X,X}(X) + f_{B_X,Y}(Y) + f_{B_X,Z}(Z) \\ B_{Y,stat}(\boldsymbol{X}) &= f_{B_Y,X}(X) + f_{B_Y,Y}(Y) + f_{B_Y,Z}(Z) \\ B_{Z,stat}(\boldsymbol{X}) &= f_{B_Z,X}(X) + f_{B_Z,Y}(Y) + f_{B_Z}(X,Y,Z) \end{aligned}$$

where $f_{B_X,X}$, $f_{B_X,Y}$ et cetera are analytical functions [1].

1.1 Measurement of an Indoor Stationary Magnetic Field

An estimation of the spatial course of the three components of an indoor magnetic field is difficult to substantiate wherefore it is determined by measurements. One obtains :

$$f_{B_X,X}(X) + f_{B_X,Y}(Y), \quad f_{B_Y,X}(X) + f_{B_Y,Y}(Y) \quad \text{and} \quad f_{B_Z,X}(X) + f_{B_Z,Y}(Y)$$

in an area of 2 m by 0.5 m . Due to the lack of test facilities $f_{B_Z,X}(Z)$ and $f_{B_Z,Y}(Z)$ had to be estimated. $f_{B_Z}(X,Y,Z)$ is then given by the Gauss's law for magnetism, that is

$$\nabla \cdot \boldsymbol{B} = 0$$

1.1.1 Experimental Setup and Execution

For the measuring series a magnetometer sensor (see [2]) was fixed on a slide, which can be manually moved on a rail of 0.51 m in effective length. This (auxiliary) rail in turn is bolted onto another slide, whose position, velocity and acceleration can be controlled by computer. The corresponding (main) rail has a usable length of 2 m. Both rails are parallel

1. This assumption allows the calculation of the magnetic as an analytic function ; for this reason the counter variable j is omitted

Travaux réalisés par le Centre Automatique et Systèmes (CAS) commun à ARMINES et Mines ParisTech dans le cadre de la procédure RAPID, projet Lorelei financé par la DGCIS

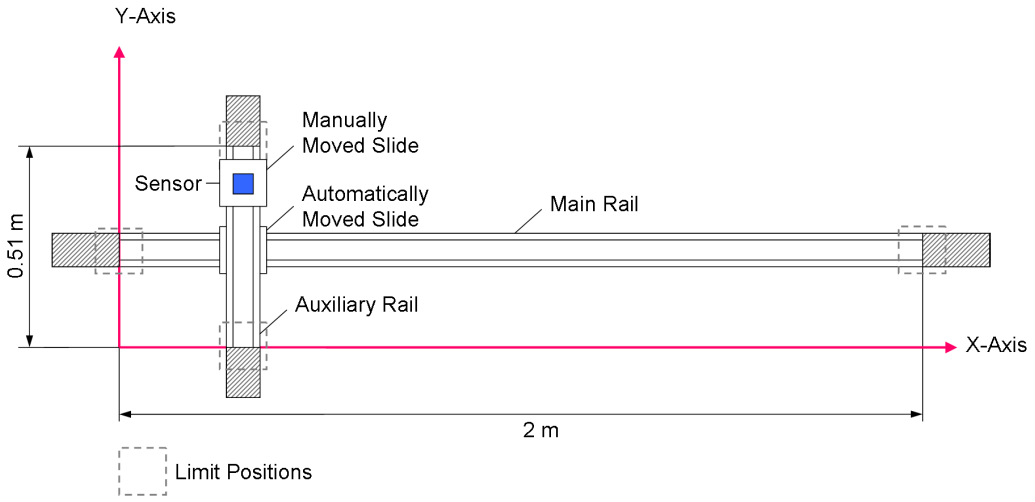

FIGURE 1 – Sketch of the experimental setup

to the ground and, more importantly, perpendicular to each other. For this reason, the X-axis and the Y-axis used below are chosen as such that they are parallel to the rails, see figure 1.
The velocity profile of the automatically moved slide, that was used for the measurements is shown in figure 2. After a waiting period of 60 s at the initial position $X = 0$ m the velocity increases to 1 m/s with a prompt acceleration of 10 m/s^2 and remains constant afterwards. At the end of the main rail, videlicet at $X = 2$ m, the slide decelerates with -10 m/s^2 and the velocity goes back to zero. Following a delay of 90 s the velocity further decreases to -1 m/s with -10 m/s^2, meaning the slide is moving in the negative X-axis direction. When the initial position is reached again, the slide stops, as a matter of course also with 10 m/s^2. The delay between the outward and return tour differs from the waiting time in the initial position to facilitate the data evaluation.
The velocity was set to 1 m/s, respectively -1 m/s in order to have equidistantly distributed measurement points. The sample frequency of the sensor is 100 Hz. In consequence, there are 200 measurement points in X-axis direction at a distance of 0.01 m (at constant Y). However, the few supernumerary data emerging from the extremely fast acceleration and deceleration processes needed to be eliminated.
Because of the shortness of the auxiliary rail and due to the fact that the second slide had to be manually moved, there are only 17 measurement points at a distance of 3 cm in direction of the Y-axis (for constant X). In sum, this leads to grid of $200 \times 17 = 3400$ measurement points.

As magnetic fields are very difficult to shield, an important point in the execution of the measurements was to eliminate possible time-dependant components. For each Y-position the velocity cycle described above was run 10 times at different intervals, delivering 10×2 measurement values for each individual point. The resulting superposition of the relevant sections is exemplary shown in figure 3 for $Y = 9$ cm; naturally the measurement graphs were flipped for the second part of the velocity cycle. The arithmetic mean calculated over

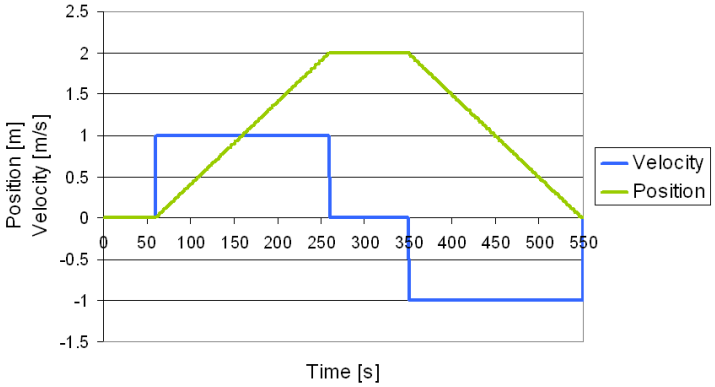

FIGURE 2 – Velocity profile used for the indoor magnetic field measurements and position of the main slide

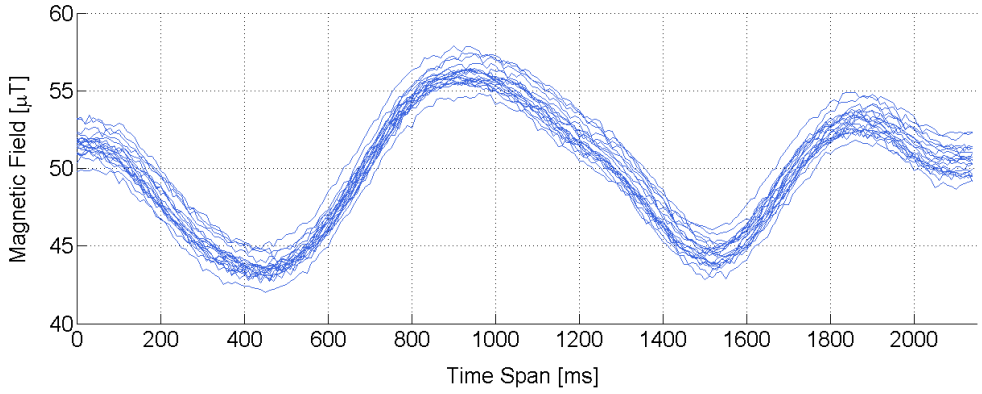

FIGURE 3 – Superposition of the repeated magnetic field measurements at changing X and constant $Y = 9$ cm

these data :

$$\boldsymbol{B}(X,Y) = \begin{pmatrix} \bar{B}_X(X,Y) \\ \bar{B}_Y(X,Y) \\ \bar{B}_Z(X,Y) \end{pmatrix} = \frac{1}{20} \cdot \sum_{j=1}^{20} \begin{pmatrix} B_{X,j}(X,Y) \\ B_{Y,j}(X,Y) \\ B_{z,j}(X,Y) \end{pmatrix}$$

is assumed to describe the stationary indoor magnetic field in the examined area.

1.1.2 Results and Evaluation

Figure 4, figure 5 and figure 6 show in their top subfigure the measured spacial course of the stationary X-, Y- and Z-component of the examined indoor magnetic field. The bottom subfigure illustrates the corresponding simulation calculated by :

$$\begin{aligned} \bar{B}_X(X,Y) =& 35\ \mu\mathrm{T} \cdot \sin\left(2\pi \cdot \frac{0.8 \cdot X}{m} - \frac{\pi}{10}\right) \\ &+ 150\ \mu\mathrm{T} \cdot \sin\left(2\pi \cdot \frac{0.8 \cdot Y}{m} + \frac{7\pi}{9}\right) + 185\ \mu\mathrm{T} \end{aligned} \tag{1}$$

$$\begin{aligned}\bar{B}_Y(X,Y) =& 45\ \mu\mathrm{T}\cdot\sin\left(2\pi\cdot\frac{X}{\mathrm{m}}-\frac{6\pi}{10}\right)\\ &+60\ \mu\mathrm{T}\cdot\sin\left(2\pi\cdot\frac{1.2\cdot Y}{\mathrm{m}}+\frac{5\pi}{9}\right)-30\ \mu\mathrm{T}\end{aligned}\tag{2}$$

$$\begin{aligned}\bar{B}_Z(X,Y) =& 50\ \mu\mathrm{T}\cdot\sin\left(2\pi\cdot\frac{X}{\mathrm{m}}+\frac{7\pi}{9}\right)\\ &+50\ \mu\mathrm{T}\cdot\sin\left(2\pi\cdot\frac{1.4\cdot Y}{\mathrm{m}}+\frac{\pi}{10}\right)+455\ \mu\mathrm{T}\end{aligned}\tag{3}$$

The X-dependent parts of the identified formulas (1), (2) and (3) were determined by Fourier transform ; the Y-dependant part had to be approximated due to an insufficient number of measurement points. The sinusoidal form of the functions was obvious from the measurements, see figure 3.

1.2 Simulation of a Stationary Indoor Magnetic Field

The equations (1) to (3) are determined on the basis of an area of 2 by 0.5 m. Nevertheless, it is assumed that they are true for the whole magnetic field the later introduced trajectory lies in. Defining that the measurements were conducted at $Z = 0$, we obtain for the analytical functions describing $B_{X,stat}(\boldsymbol{X})$, $B_{Y,stat}(\boldsymbol{X})$ and $B_{Z,stat}(\boldsymbol{X})$:

$$\begin{aligned}f_{B_X,X}(X) &= 35\ \mu\mathrm{T}\cdot\sin\left(2\pi\cdot\frac{0.8\cdot X}{\mathrm{m}}+\Delta\varphi_{B_X,X}\right)\\ f_{B_X,Y}(Y) &= 150\ \mu\mathrm{T}\cdot\sin\left(2\pi\cdot\frac{0.8\cdot Y}{\mathrm{m}}+\Delta\varphi_{B_X,Y}\right)\\ f_{B_Y,X}(X) &= 45\ \mu\mathrm{T}\cdot\sin\left(2\pi\cdot\frac{X}{m}+\Delta\varphi_{B_Y,X}\right)\\ f_{B_Y,Y}(Y) &= 60\ \mu\mathrm{T}\cdot\sin\left(2\pi\cdot\frac{1.2\cdot Y}{\mathrm{m}}+\Delta\varphi_{B_Y,Y}\right)\\ f_{B_Z,X}(X) &= 50\ \mu\mathrm{T}\cdot\sin\left(2\pi\cdot\frac{X}{\mathrm{m}}+\Delta\varphi_{B_Z,X}\right)\\ f_{B_Z,Y}(Y) &= 50\ \mu\mathrm{T}\cdot\sin\left(2\pi\cdot\frac{1.4\cdot Y}{\mathrm{m}}+\Delta\varphi_{B_Z,Y}\right)\end{aligned}$$

However, as already mentioned, $f_{B_X,Z}(Z)$, $f_{B_Y,Z}(Z)$ and $f_{B_Z}(X,Y,Z)$ could not be determined by the experiment. With the help of the following two non-verifiable presumptions :

1. The "frequency" of the Z-dependent sinus function is the arithmetic mean of the frequencies of the X- and Y-dependent functions.
2. The constant summands of equation (1) and equation (2) are presumed to be the effective value of the Z-dependent sinus function. The "amplitude" thus results from the multiplication with $\sqrt{2}$.

we find :

$$\begin{aligned}f_{B_X,Z}(Z) &= 254\ \mu\mathrm{T}\cdot\sin\left(2\pi\cdot\frac{0.8\cdot Z}{\mathrm{m}}+\Delta\varphi_{B_X,Z}\right)\\ f_{B_Y,Z}(Z) &= -42\ \mu\mathrm{T}\cdot\sin\left(2\pi\cdot\frac{1.1\cdot Y}{\mathrm{m}}+\Delta\varphi_{B_Y,Z}\right)\end{aligned}$$

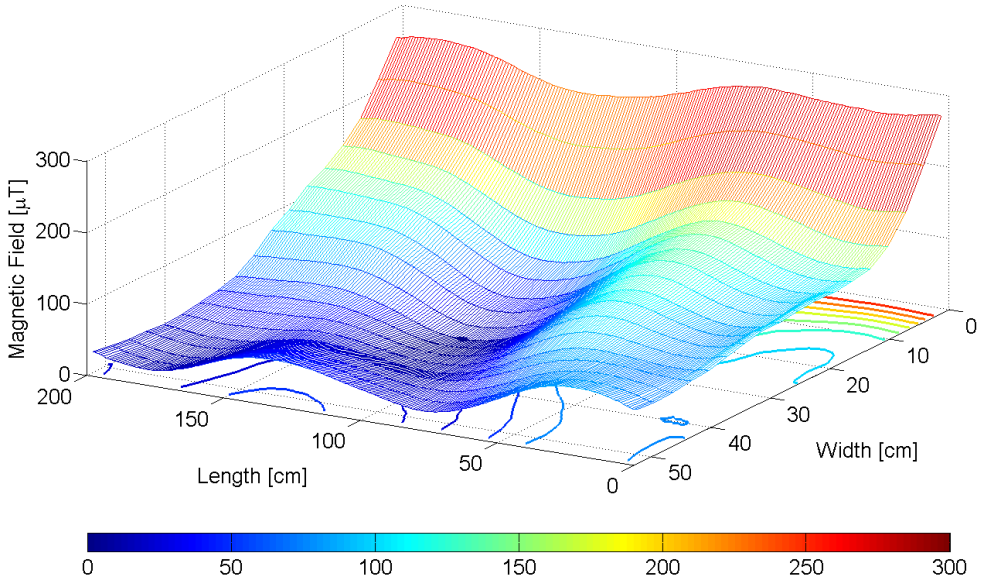

(a) Measurement results

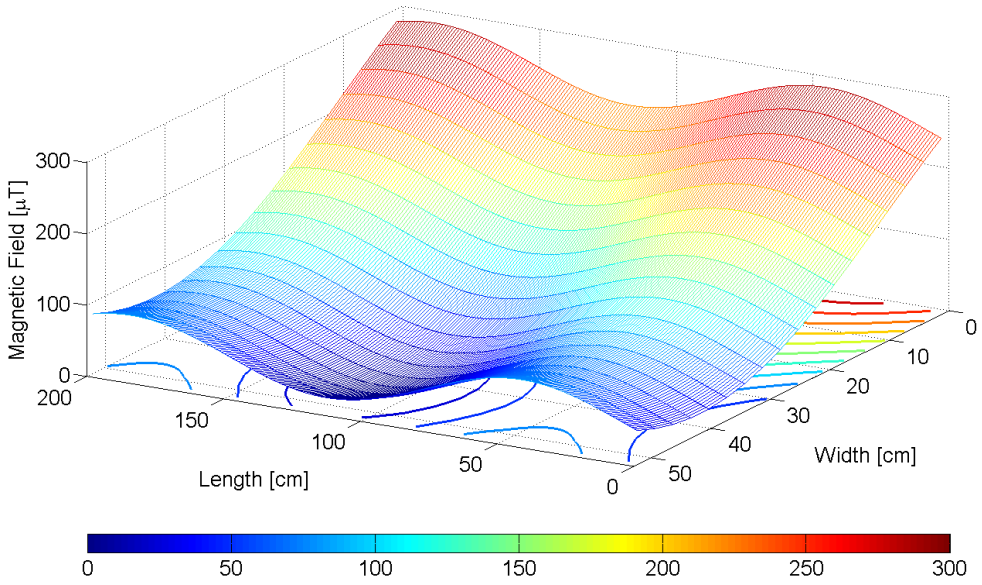

(b) Simulation

FIGURE 4 – Spatial course of the X-component of a stationary indoor magnetic field

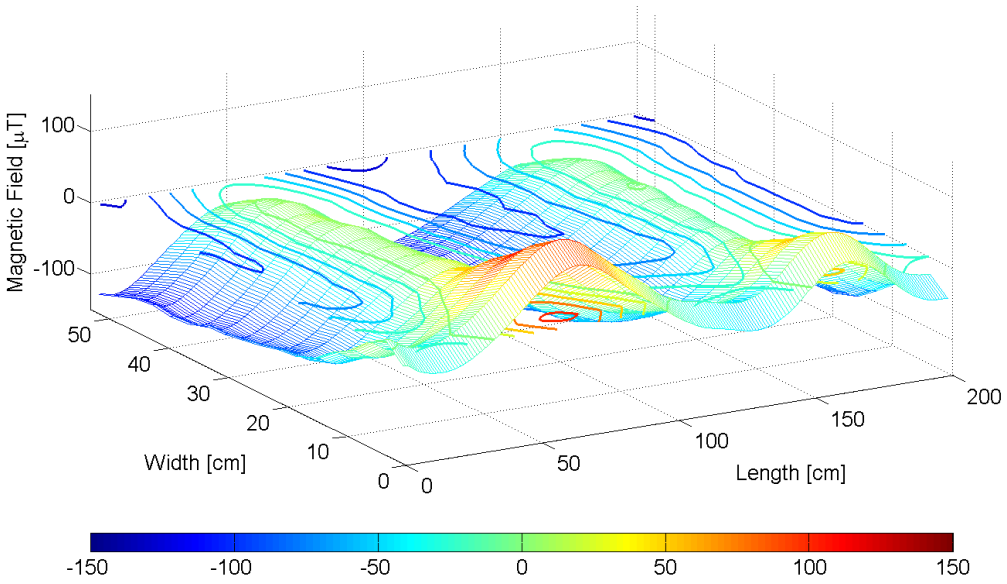

(a) Measurement results

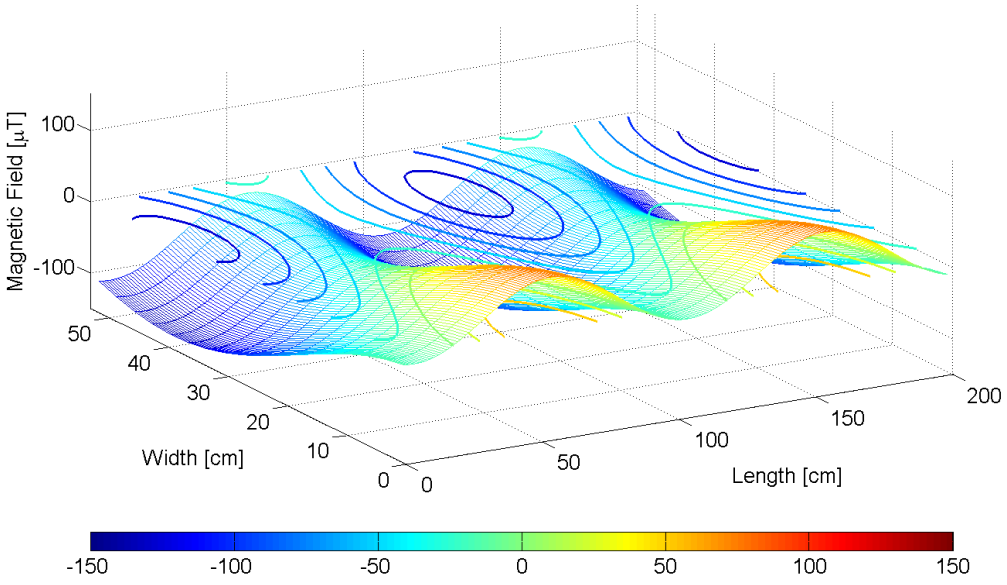

(b) Simulation

FIGURE 5 – Spatial course of the Y-component of a stationary indoor magnetic field

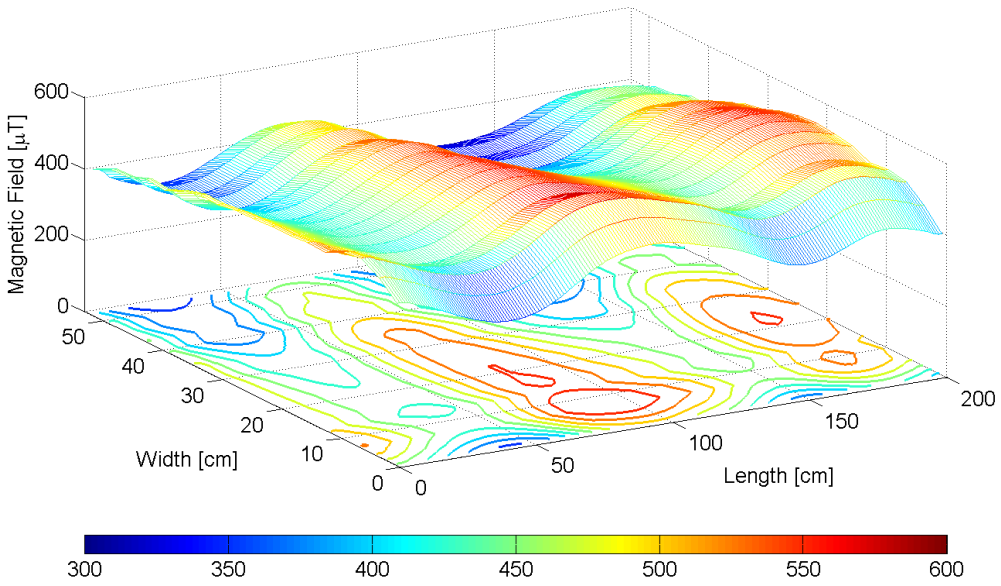

(a) Measurement results

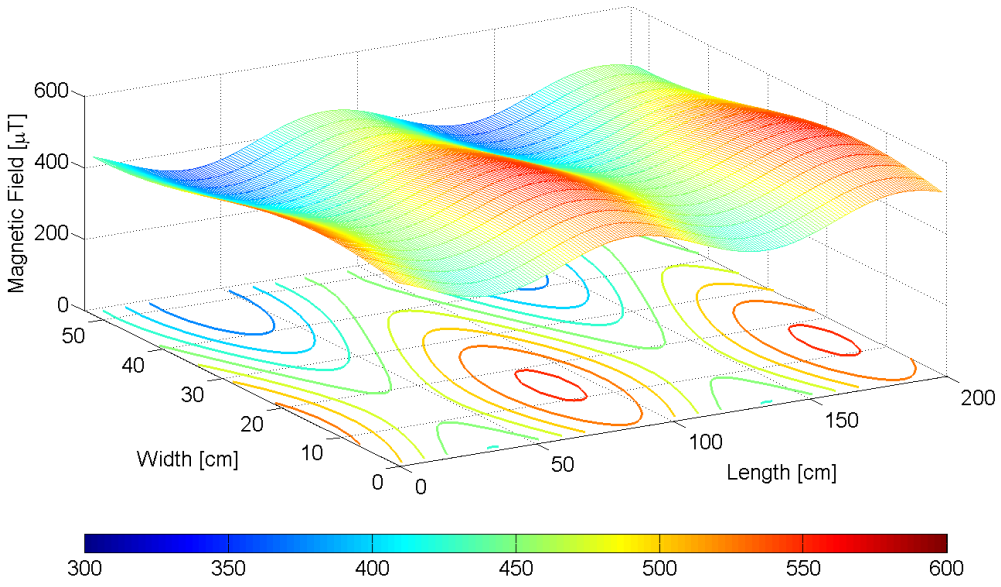

(b) Simulation

FIGURE 6 – Spatial course of the Z-component of a stationary indoor magnetic field

TABLE 1 – Phase shifts for the sinus functions describing the stationary indoor magnetic field

$\Delta\varphi_{B_X,X}$	4.9	$\Delta\varphi_{B_Y,X}$	2.4	$\Delta\varphi_{B_Z,X}$	1.5
$\Delta\varphi_{B_X,Y}$	2.5	$\Delta\varphi_{B_Y,Y}$	0.6	$\Delta\varphi_{B_Z,Y}$	0.8
$\Delta\varphi_{B_X,Z}$	5.9	$\Delta\varphi_{B_Y,Z}$	6.0		

Ultimately, $f_{B_Z}(X,Y,Z)$ is defined by Gauss's law for magnetism :

$$\begin{aligned} 0 &\stackrel{!}{=} \nabla \cdot \boldsymbol{B} = \frac{\partial B_X}{\partial X} + \frac{\partial B_Y}{\partial Y} + \frac{\partial B_Z}{\partial Z} \\ \Rightarrow \quad 0 &\stackrel{!}{=} \frac{\partial f_{B_X,X}(X)}{\partial X} + \frac{\partial f_{B_Y,Y}(Y)}{\partial Y} + \frac{\partial f_{B_Z,Z}(Z)}{\partial Z} \end{aligned}$$

This yields :

$$\begin{aligned} f_{B_Z}(X,Y,Z) = &- \int 35\ \mu T \cdot \cos\left(2\pi \cdot \frac{0.8 \cdot X}{\mathrm{m}} + \Delta\varphi_{B_X,X}\right) \cdot 2\pi \cdot 0.7 \cdot \mathrm{d}Z \\ &- \int 60\ \mu T \cdot \cos\left(2\pi \cdot \frac{1.2 \cdot Y}{\mathrm{m}} + \Delta\varphi_{B_Y,Y}\right) \cdot 2\pi \cdot 1.2\mathrm{d}Z \\ = &- \left[35\ \mu T \cdot \cos\left(2\pi \cdot \frac{0.8 \cdot X}{\mathrm{m}} + \Delta\varphi_{B_X,X}\right) \cdot 2\pi \cdot 0.7\right] \cdot Z \\ &- \left[60\ \mu T \cdot \cos\left(2\pi \cdot \frac{1.2 \cdot Y}{\mathrm{m}} + \Delta\varphi_{B_Y,Y}\right) \cdot 2\pi \cdot 1.2\right] \cdot Z \end{aligned}$$

The phase-shifts of equation (1) to equation (3) were selected in such a way that the magnetic field in the relevant section is equal to the measurements. In reality, the phase-shifts, denoted with $\Delta\varphi_{B_X,X}$ etc., depend completely on the start position within the magnetic field. For this reason, they are randomly chosen between 0 and 2π, taking the values shown in table 1.

2 Presence of Magnetic Disturbances

In the presence of transient magnetic disturbances, their time-dependent equations have to be added to the stationary magnetic field of chapter 1. This yields :

$$\boldsymbol{B}(\boldsymbol{X},t) \quad = \quad \boldsymbol{B}_{stat}(\boldsymbol{X}) + \boldsymbol{B}_{trans}(\boldsymbol{X},t)$$

There are two main models describing transient magnetic fields : the oscillating magnetic dipole and the straight wire carrying a time-dependent current. They are given below.

2.1 The Oscillating Magnetic Dipole

The magnetic field of the oscillating magnetic dipole can be described through the following set of equations :

$$\begin{aligned}
\boldsymbol{B}_{dip}\left(\boldsymbol{X},t\right) &= Re\left(\mu_0\mu_r \cdot \frac{e^{ik\cdot|\boldsymbol{r}|}}{4\pi\cdot|\boldsymbol{r}|^3}\cdot\left[3\cdot\boldsymbol{e}_r\cdot\{\boldsymbol{e}_r\cdot\boldsymbol{m}(\theta,\psi,t)\}-\boldsymbol{m}(\theta,\psi,t)\right]\right)\\
\boldsymbol{m}(\theta,\psi,t) &= \boldsymbol{R}(\theta,\phi)\cdot\begin{pmatrix}M\cdot\cos(2\pi\cdot f\cdot t+\Delta\varphi)\\0\\0\end{pmatrix}\\
\boldsymbol{r} &= \boldsymbol{X}-\boldsymbol{X}_{dip}\\
\boldsymbol{e}_r &= \frac{\boldsymbol{r}}{|\boldsymbol{r}|}\\
k &= \frac{2\pi\cdot f}{c}
\end{aligned}$$

Apart from the variable inputs X, Y, Z and t the following parameters need to be set :

1. the position of the dipole $\boldsymbol{X}_{dip}$,
2. the two angles describing the rotational state of the dipole θ, ψ,
3. the absolute value of the magnetic dipole moment M,
4. the frequency f and the phase shift $\Delta\varphi$.

2.2 The Straight Current-Carrying Wire

The magnetic field of a straight current-carrying wire (of infinite length) can be calculated with :

$$\begin{aligned}
\boldsymbol{B}_{wire}(\boldsymbol{X},t) &= \mu_0\mu_r\cdot\frac{i(t)}{2\pi\cdot|\boldsymbol{r}|}\cdot[\boldsymbol{e_I}\times\boldsymbol{e_r}]\\
i(t) &= \hat{i}(t)\cdot\cos\left(2\pi\cdot f\cdot\left[t+\frac{|\boldsymbol{r}|}{c}\right]+\Delta\varphi\right)\\
\boldsymbol{r} &= \boldsymbol{X}-\left[\boldsymbol{X}_{wire}+\boldsymbol{e}_I\cdot\left\{\frac{\boldsymbol{e}_I\cdot(\boldsymbol{X}-\boldsymbol{X}_{wire})}{\boldsymbol{e}_I^2}\right\}\right]\\
\boldsymbol{e}_r &= \frac{\boldsymbol{r}}{|\boldsymbol{r}|}
\end{aligned}$$

Here again, some parameters need to be set aside from the variable inputs X, Y, Z and t :

1. the position and the direction vector defining the straight line, namely $\boldsymbol{X}_{wire}$ and $\boldsymbol{e}_I$,
2. the current amplitude $\hat{i}(t)$,
3. the frequency f and the phase shift $\Delta\varphi$.

2.3 The Magnetic Field $\boldsymbol{B}$

Assuming that there are n oscillating dipoles and m wires carrying a time-dependent current, the transient part $\boldsymbol{B}_{trans}(x,y,z,t)$ is represented by :

$$\boldsymbol{B}_{trans}(\boldsymbol{X},t)=\sum_{k=1}^{n}\boldsymbol{B}_{dip,k}(\boldsymbol{X},t)+\sum_{k=1}^{m}\boldsymbol{B}_{wire,k}(\boldsymbol{X},t)$$

Consequently, the total magnetic field $\boldsymbol{B}(\boldsymbol{X}, t)$ can be written as :

$$\boldsymbol{B}(\boldsymbol{X}, t) = \boldsymbol{B}_{stat}(\boldsymbol{X}, t) + \sum_{k=1}^{n} \boldsymbol{B}_{dip,k}(\boldsymbol{X}, t) + \sum_{k=1}^{m} \boldsymbol{B}_{wire,k}(\boldsymbol{X}, t) \tag{4}$$

Références

[1] M. Angermann, M. Frassl, M. Doniecy, B. Julianyz, and P. Robertson. Characterization of the indoor magnetic field for applications in localization and mapping. In *International Conference on Indoor Positioning and Indoor Navigation 2012*, 2012.

[2] Xsens-Technologies B.V. *Motion tracker B Technical Documentation*, 1.01 edition, 2002-2003.

[3] G. Zachmann. Distortion correction of magnetic fields for position tracking. In *Computer Graphics International 2007*, pages 213 – 220, 251. IEEE Computer Society Press, 2007.

A Nomenclature

A.1 Vectors and Matrices

$\boldsymbol{A}$	state matrix (state space)
$\boldsymbol{B}$	magnetic field vector in R_i
$\nabla \boldsymbol{B} = \frac{\partial \boldsymbol{B}}{\partial \boldsymbol{X}}$	Jacobian matrix of the magnetic field $\boldsymbol{B}$
$\boldsymbol{b}$	magnetic field vector in R_b
$\hat{\boldsymbol{b}}$	estimation of the magnetic field vector $\boldsymbol{b}$
$\nabla \boldsymbol{b} = \frac{\partial \boldsymbol{b}}{\partial \boldsymbol{x}}$	Jacobian matrix of the magnetic field $\boldsymbol{b}$
$\boldsymbol{C}$	output matrix (state space)
$\boldsymbol{D}$	electric flux density
$\boldsymbol{E}$	electric field (strenth)
$\boldsymbol{e}$	unit vector
$\boldsymbol{e_X}$, $\boldsymbol{e_Y}$, $\boldsymbol{e_Z}$	basis vectors of the inertial frame of reference
$\boldsymbol{e_x}$, $\boldsymbol{e_y}$, $\boldsymbol{e_z}$	basis vectors of the body frame of reference
$\boldsymbol{F}_E$	external forces
$\boldsymbol{H}$	magnetic field strength
$\boldsymbol{J}$	current density
$\boldsymbol{L}$	gain matrix
$\boldsymbol{m}$	magnetic dipole moment
$\boldsymbol{p}$, $\boldsymbol{q}$	coordinate vectors
$\boldsymbol{Q}_B$	observability matrix
$\boldsymbol{R}$	rotation matrix
$\boldsymbol{R}_b$	matrix containing the basis vectors of the body reference frame
$\boldsymbol{R}_i$	matrix containing the basis vectors of the inertial reference frame
$\boldsymbol{R}_x$, $\boldsymbol{R}_y$, $\boldsymbol{R}_z$	rotation matrices about the x-,y- and z-axis
$\boldsymbol{r}$	distance vector
$\boldsymbol{T}_{i \to b}$	transformation matrix between R_i and R_b
$\boldsymbol{V}$	velocity vector in R_i
$\hat{\boldsymbol{V}}$	estimation-based calculation of the velocity vector $\boldsymbol{V}$
$\boldsymbol{v}$	velocity vector in R_b

$\hat{\boldsymbol{v}}$	estimation of the velocity vector $\boldsymbol{v}$
$\boldsymbol{W}$	rate of turn vector in R_i
$\boldsymbol{w}$	rate of turn vector in R_b
$\boldsymbol{X}$	position vector in R_i
$\hat{\boldsymbol{X}}$	estimation-based calculation of the position vector $\boldsymbol{X}$
$\boldsymbol{x}$	position vector in R_b
$\boldsymbol{y}$	output vector (state space)
$\boldsymbol{\beta}$	magnetic field vector
$\boldsymbol{\nu}$	velocity vector
$\boldsymbol{\xi}$	position vector
$\boldsymbol{\Upsilon}$	linear transposition matrix (arbitrary)
$\boldsymbol{\chi}$	state vector
$\tilde{\boldsymbol{\chi}}$	alternative state vector
$\boldsymbol{\Omega}_W$	rotation matrix corresponding to the rate of turn vector $\boldsymbol{W}$
$\boldsymbol{\Omega}_w$	rotation matrix corresponding to the rate of turn vector $\boldsymbol{W}$
$\boldsymbol{\omega}$	rate of turn vector

A.2 Scalars, Functions and Sets

$B_x,\ B_y,\ B_z$	coordinates of $\boldsymbol{B}$, the magnetic field vector in R_i
$b_x,\ b_y,\ b_z$	coordinates of $\boldsymbol{b}$, the magnetic field vector in R_b
$\hat{b}_x,\ \hat{b}_y,\ \hat{b}_z$	coordinates of $\hat{\boldsymbol{b}}$, the estimated magnetic field vector
C	substation charge
f	frequency
f	analytic function
h	auxiliary function
I	current
k	wave number
L	motor load
l	length
$l_1,\ l_2$	constant gains of the gain matrix $\boldsymbol{L}$
M	magnetic dipole moment (absolute value)
$n,\ m$	quantities
$P,\ Q,\ R$	coordinates of $\boldsymbol{W}$, the rate of turn vector in R_i
$p,\ q,\ r$	coordinates of $\boldsymbol{w}$, the rate of turn vector in R_b
r	distance
$\Re_b$	body reference frame
R_b	basis of the body reference frame
$\Re_i$	inertial reference frame
R_i	basis of the inertial reference frame
t	time
t_0	start time
Δt	discrete time step, reciprocal of the sample frequency
$U,\ V,\ W$	coordinates of $\boldsymbol{V}$, the velocity vector in R_i
$\hat{U},\ \hat{V},\ \hat{W}$	coordinates of $\hat{\boldsymbol{V}}$, the estimation-based calculation of the velocity vector in R_i
$u,\ v,\ w$	coordinates of $\boldsymbol{v}$, the velocity vector in R_b
$\hat{u},\ \hat{v},\ \hat{w}$	coordinates of $\hat{\boldsymbol{v}}$, the estimated velocity vector in R_b
V	Lyapunov candidate function
$X,\ Y,\ Z$	coordinates of $\boldsymbol{X}$, the position vector in R_i

$\hat{X},\ \hat{Y},\ \hat{Z}$	coordinates of $\hat{\boldsymbol{X}}$, the estimation-based calculation of the position vector in R_i
$x,\ y,\ z$	coordinates of $\boldsymbol{x}$, the position vector in R_b
$x,\ y,\ z$	Cartesian coordinates
α	auxiliary angle
ε_0	electric constant
ε_r	relative electric permittivity
μ_0	magnetic constant
μ_r	relative magnetic permeability
ρ	volume charge density
φ	angle of the right triangle defined by the Cartesian coordinates x (opposite leg) and z (adjacent leg)
$\Delta\varphi$	phase shift
$\phi,\ \theta,\ \psi$	set of angles describing a rotational state
ω	angular velocity

A.3 Indices

avg	average
b	body
cat	catenary
dip	dipole
dir	direction
e	estimation
eff	effective
f	final
$gyro$	gyrometer
I	current
i	inertial
$j,\ k$	counter variable
m	measured
$magneto$	magnetometer
max	maximum
min	minimum
MV	mean value
p	prediction
r	distance
s	sensor
sp	sample
$stat$	stationary
t	trains
$trans$	transient
w	wire
$X,\ Y,\ Z$	component in X-, Y- and Z-axis direction
$x,\ y,\ z$	component in x-, y- and z-axis direction

A.4 List of Abbreviations

AC	Alternating Current

AWGN	Additive White Gaussian Noise
CAS	*Centre Automatique et Systèmes*
DC	Direct Current
IRT	*Institut für Regelungstechnik*
PSU	Power Supply Unit
RATP	*Régie Autonome des Transports Parisiens*
RER	*Réseau Express Régionale*
RMS	Root Mean Square
SNCF	*Société Nationale des Chemins de Fer Français*
TGV	*Train à Grance Vistesse*